A capacitance-based micropositioning system for x-ray rocking curve measurements

G. L. Miller, R. A. Boie, P. L. Cowan, J. A. Golovchenko, R. W. Kerr, and D. A. H. Robinson

Bell Laboratories, Murray Hill, New Jersey 07974

(Received 14 March 1979; accepted for publication 4 May 1979)

Certain types of x-ray experiments require very precise angular positioning of crystals in the vicinity of the Bragg reflection condition. A system applicable to some measurement of this type is described which achieves a long-term angular stability of $\sim 10^{-7}$ radians, coupled with a linear angular readout. This is achieved through a novel capacitance sensing system which provides angle measurement, together with the use of an auxilliary servo loop based on the Bragg condition to ensure long-term overall angular stability.

INTRODUCTION

Numbers of interesting physical effects can occur in the vicinity of the Bragg condition.[1-5] However, experiments involving such phenomena impose substantial demands on the long-term angular stability of the systems involved.

The simplest method of providing such stability is by the use of suitably massive and rigid mechanical supports together with an appropriate degree of overall temperature control. However, while this can be a satisfactory approach, it is necessarily bulky, relatively expensive, and can involve inconveniently long thermal time constants.

An alternative method is presented here in which a crystal is repetitively swept through the Bragg condition in a time short compared to the system thermal time constants or mechanical drift times. This approach is specifically intended for experiments of the type described in Ref. 2 in which one is concerned both with stabilizing and measuring the position of the x-ray standing-wave field inside a target crystal. The instantaneous angular position of the crystal is sensed capacitively, while the true zero position of the system is constantly updated by repetitively noting the position of the centroid of the x-ray rocking curve itself. An overall block diagram is shown in Fig. 1.

A PZT crystal element (Burleigh Industries No. PZ-40) is used to rotate the rocking crystal, such as to sweep it through the Bragg condition every few seconds. However, as will be demonstrated in Sec. I, the drive voltage to such crystals is not a reliable measure of their dimensions. The instantaneous angular position of the crystal is therefore measured by means of capacitor pick-off plates mounted directly on the PZT transducer housing as indicated in Fig. 2. While it is readily demonstrated that the sensitivity of such capacitive-distance sensors is proportional to the reciprocal of the air gap, this sensitivity improvement is usually accompanied by an increasingly nonlinear readout. This remains true both for the usual systems that sense the rf displacement current of the capacitor directly and for more sophisticated bridge configurations.[6]

To overcome this limitation (an important one in this and many other distance measuring applications), a new form of capacitance-distance measuring scheme has

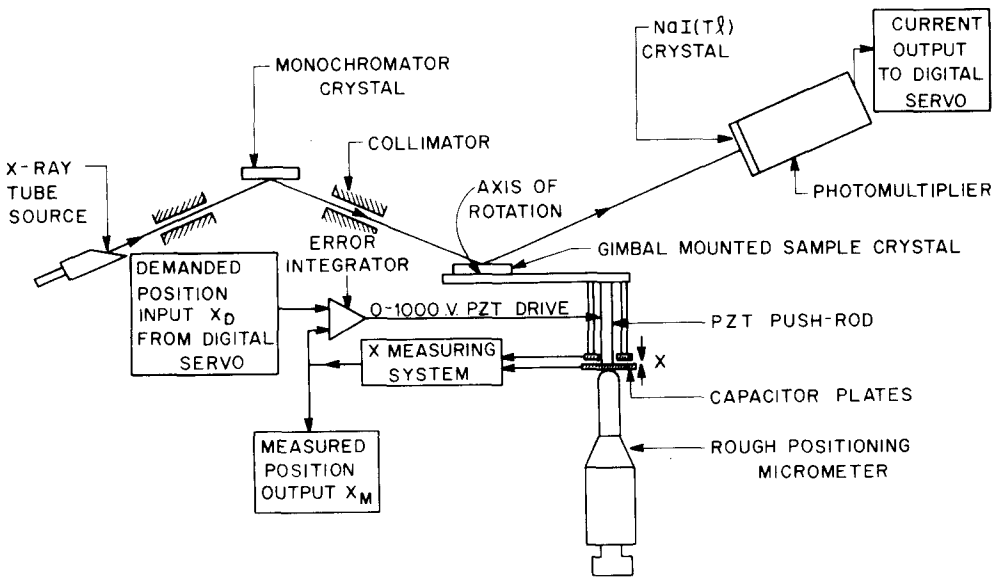

FIG. 1. Overall block diagram of the x-ray rocking curve system.

 0034-6748/79/091062-08$00.60

been devised. This is described in detail in Sec. I and provides an inherently linear readout with distance over the entire available motion of the PZT transducer. The linearity is better than 1% while the measured positional noise is less than 100 Å.

The distance measuring system is incorporated inside a larger feedback loop, as indicated in Fig. 1, to provide a position-following capability. A separate servo, described in Sec. II, provides a repetitive triangular input waveform to the distance measuring loop. Long-term stability is assured by monitoring the Bragg reflection condition on each sweep through the rocking curve by means of a NaI (Tl) scintillation counter. A small correction is made at the end of each sweep in such a way as to maintain the centroid of the rocking curve precisely in the middle of the angular range.

I. DISTANCE MEASUREMENT

The basic linearity problem with existing capacitance transducers for position determination is that they measure the rf current flowing through the capacitor of interest at a *fixed* rf voltage. This leads to a hyperbolic relation between capacitor plate spacing and output signal. While this condition can be ameliorated by the use of a more complicated transducer configuration, employing a moving plate between two fixed ones,[6] this still only provides a readout that is linear to first order.

An obvious improvement can be effected by using the capacitance element in the feedback loop of an operational integrator, and driving the integrator from a constant-current rf generator. It is evident that the rf voltage appearing at the integrator output should then be proportional to the spacing of the capacitor plates.

While this scheme is superficially attractive, it turns out to exhibit some drawbacks. Central among these are the facts that the operational integrator suffers from widely varying reserve gain as the capacitor plates traverse large distances and that in addition the system requires the use of an exceedingly linear rf rectifier to provide the final position information.

A superior approach, retaining all of the integrator's advantages in addition to adding some others, can instead be realized by means of the scheme shown in Fig. 3.

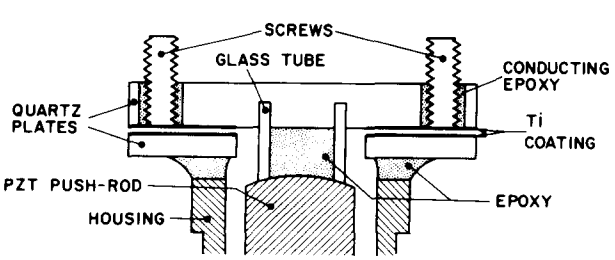

FIG. 2. Cross-sectional view of the distance measuring capacitor plates mounted on the PZT transducer. The lower quartz plate is metallized in a complete annulus, while the upper metallization is segmented into two equal semicircular regions. The midrange spacing and capacitance are ~20 μm and ~20 pF, respectively.

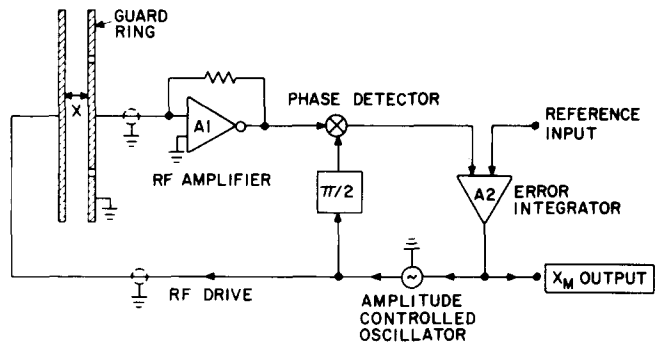

FIG. 3. Simplified block diagram of the linear distance measuring system.

Here the rf current flowing through the distance measuring capacitor is monitored by a current amplifier A1 followed by a synchronous detector. The detector output is compared with a fixed reference voltage and any error between the two is integrated by A2. The output of A2 is then used to control the amplitude of the oscillator that provides the rf drive to the capacitor. It is evident that this regime automatically adjusts the oscillator amplitude so as to provide a constant displacement current through the capacitor, thereby ensuring that the oscillator amplitude is itself proportional to the distance X.

Enumeration of the specific advantages of this approach will be postponed until the details of the method have been described. However, it is worth noting at this point that, provided there exists a linear relation between the A2 output and the oscillator amplitude, the measured distance output X_M is inherently proportional to the distance X. Furthermore, it is clear that since the A1 input is itself a virtual ground, a guard ring can readily be incorporated in the capacitance transducer if desired as shown in Fig. 3 (although this refinement was not actually employed in the present case exemplified by Fig. 2). The implementation of the scheme of Fig. 3 involves a number of special considerations which are described in the ensuing more-detailed account of the design.

The rf current amplifier A1 of Fig. 3 comprises the grounded base transistor Q7 of Fig. 4, together with amplifiers A4 and A5. The latter are arranged to provide an ~45° phase shift each in order to obtain a 90° overall phase shift. The two amplifier stages are separated by a current limiter to ensure that the receiver maintains phase stability even under heavy overload conditions (omission of this feature can lead to the system locking up in certain situations). Synchronous detection is provided by Q8 through Q11, while A6 is the error integrator. The output of A6 is the integral of the difference of the rectified rf current and a preset current derived from the Zener reference.

The amplitude-controlled oscillator of Fig. 3 is implemented by the system shown in Fig. 5. Here Q3 and Q4 form an emitter-coupled multivibrator that drives the current steering long-tail pair Q2, Q5. The emitter current of Q2, Q5 is controlled by the output of the

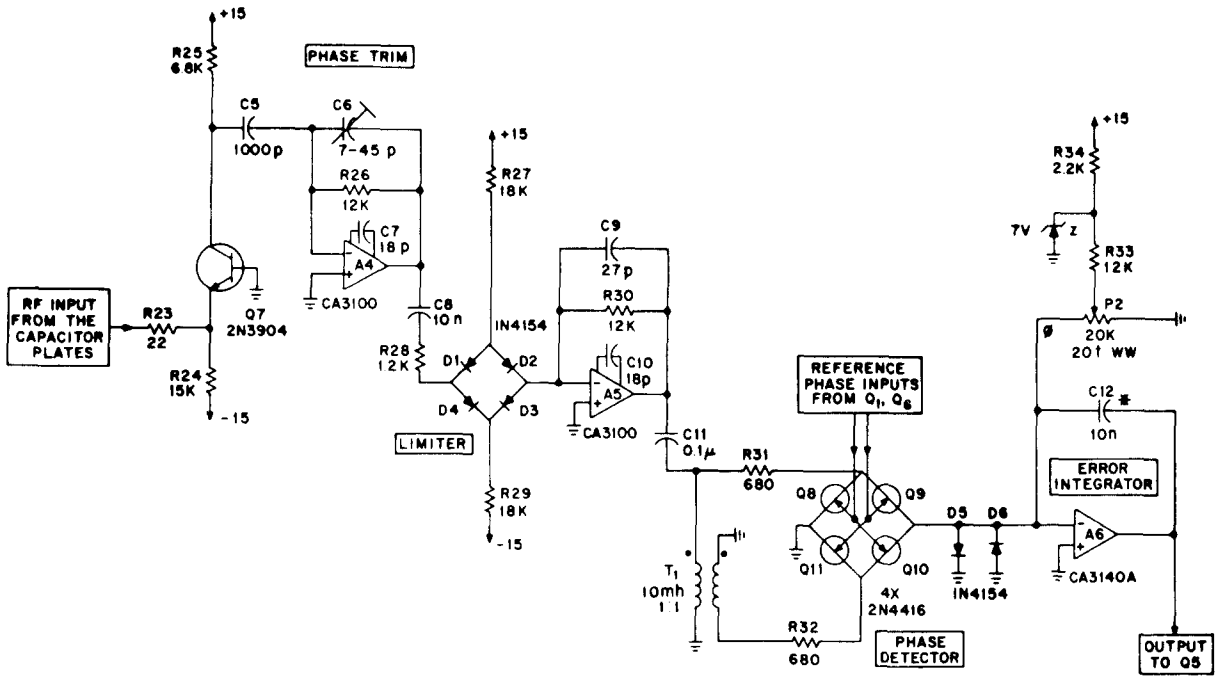

FIG. 4. Schematic of the rf amplifier and phase detector.

error integrator A6 of Fig. 4, and this current is switched between the junction of R14, R15 and R16, R17 in each half-cycle. On the other hand, the total magnitude of this switched current is clearly proportional to the essentially constant current flowing from the junction of R15, R16 into A1. The highly stable tank circuit L1, R18, C4 utilizes a dust-iron-cored inductor and is tuned to the multivibrator frequency. In this way the rf output of A3 remains accurately proportional to the dc output of A1. Furthermore, this condition clearly holds inde-

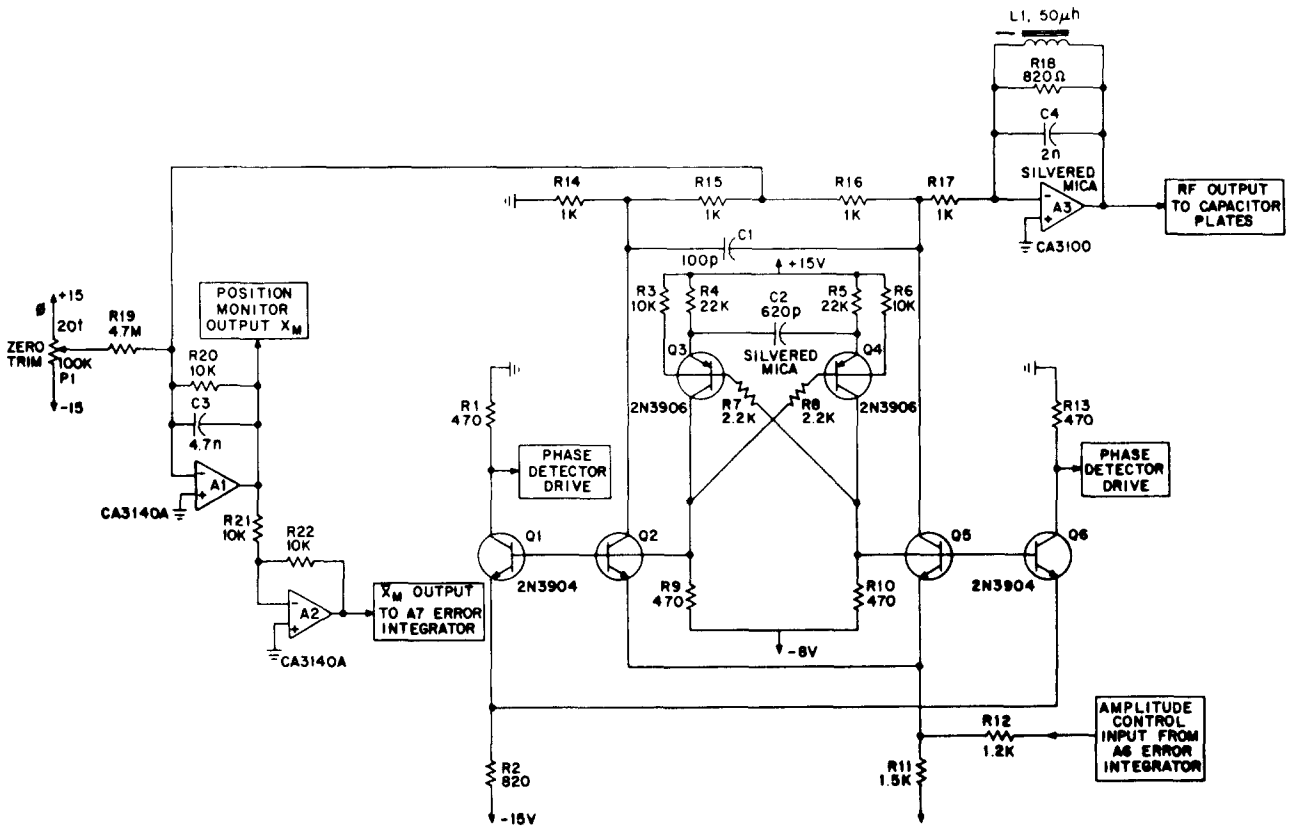

FIG. 5. Schematic of the amplitude-controlled oscillator.

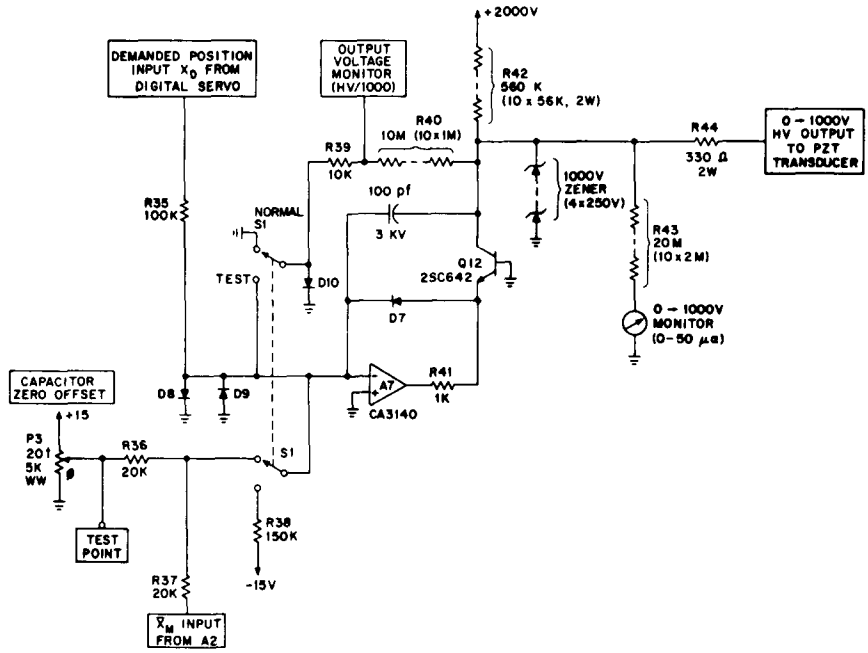

FIG. 6. Schematic of the high-voltage PZT driver amplifier.

pendent of the drive amplitude itself, and is also independent of changes in the current gains of Q2 and Q5 with current and temperature, etc. (For very demanding applications these two transistors could advantageously be a monolithic matched dual pair.)

Of course, there are numerous other ways in which such an amplitude-controlled oscillator can be realized. However, the basis of the method used here, namely that of first chopping a direct current to provide pulsating dc and then measuring its average value afterwards, offers significant advantages in terms of linearity and fast overall response, together with the avoidance of the need for a wide-range linear rectifier. The oscillator, rf receiver, rectifier, and error integrator of Fig. 4 constitute the distance measuring system.

It is appropriate to note a number of features of this approach which make it particularly suitable for such measurements. First, it is obviously wide range and inherently linear (unlike the usual fixed drive amplitude capacitor systems); second, it operates at fixed reserve gain (unlike the integrator method); third, the rf receiver and rectifier always operate with a constant signal amplitude (thereby imposing essentially no linearity demands on these elements); and finally, the receiver can incorporate a limiter with no penalty in overall system linearity. (Additional features realized by this approach are the possible use of long coaxial cables between the electronics and the capacitance sensor as well as the employment of guard-ring geometries. Although not employed here, it is also clear that essentially identical electronics could be used for high-resolution measurements over large distances [e.g., meters] by the use of different sensors such as long precision piston capacitors, etc.)

Returning to Fig. 1, it will be noted that the distance measuring system actually incorporates the PZT crystal inside a larger feedback loop to provide a position following capability. The remaining elements needed to achieve this are shown in Fig. 6, which essentially depicts a 0–1000-V operational integrator.

Any difference between the demanded position signal X_D and the measured position signal X_M is amplified by A7 in conjunction with Q12, and thereby provides the required high-voltage drive signal for the PZT transducer. Switch S1 disables the servo and allows the amplifier to provide a simple gain of $\times 100$. (This facility is useful for setup and debugging operations.)

Given the complete PZT transducer and distance measuring system comprising the elements of Figs. 2–6, it was then possible to check its performance by applying a series of known voltages X_D and measuring the corresponding values of X_M. The results of such a test are plotted in Fig. 7 and show the linearity to be better than ~0.1% over the quoted range. Additional calibrations of a similar nature were carried out by substituting ac-

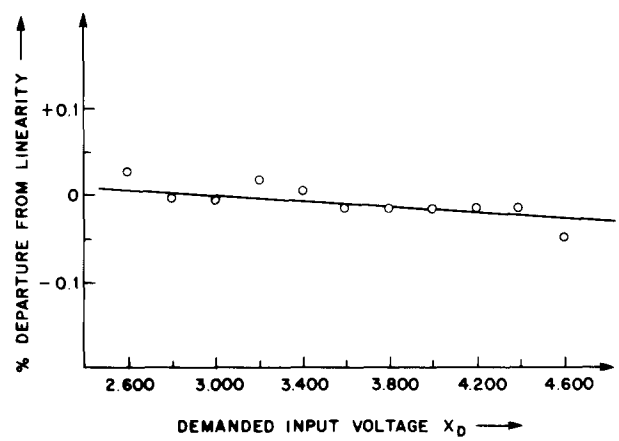

FIG. 7. Measured tracking error between the demanded and measured distance signals.

curately known capacitors for the distance measuring element.

In the course of such tests it was observed that, perhaps contrary to intuition, the parallelism of the capacitor plates is of substantial importance in respect to the system linearity. To first order it can be shown that a small relative tilt only introduces an offset in the distance measurement (which is of no significance for the present application by virtue of the action of the digital servo described in Sec. II). To second order, however, such effects can produce a nonlinear response.

In order to minimize such errors the system of Fig. 2 was assembled with a thin Mylar-foil spacer between the capacitor plates while the epoxy cured. (In retrospect, a superior design for such a pickoff would probably be some sort of flexing beam supported at each end with a thin insulating spacer. Such a design would help to maintain parallelism at all times. However, while such improvements might be worthwhile for other applications, the performance of the capacitor of Fig. 2 was judged to be adequate for the present case.)

Having checked the linearity of the distance measuring system it was then possible to investigate the behavior of the PZT element itself as a function of applied voltage over the range 100–900 V. This resulted in a minimum-to-maximum motion of ~15 to ~25 μ (i.e., ~80 V/μ) with a linearity as shown in Fig. 8.

Three points are immediately apparent: the PZT element response is nonlinear, exhibits substantial hysteresis, and does not close on itself, i.e., it exhibits memory effects. These results indicate the undesirability of attempting to use the PZT voltage-dimension relation for any accurate determination of position.

II. AVERAGE POSITION SERVO SYSTEM

While the previously described distance measuring system provides instantaneous angular information it actually only does so relative to the PZT transducer housing, which is obviously not an absolute reference. For this reason a subsidiary servo loop was employed to constantly center the x-ray rocking curve in the middle of the angular sweep of the moving crystal. This was achieved using a NaI (Tl) scintillation counter to monitor the rocking curve (as shown in Fig. 1) and by feeding the PMT anode current into the system (shown in simplified form in Fig. 9).

Here a clock oscillator drives an up–down counter and DAC, thereby providing a repetitive staircase function that approximates a smooth symmetrical triangular waveform. The PMT anode current is integrated until the scaler is half-full (i.e., the x signal output is halfway through its sweep), following which the PMT anode current is subtracted from the same integrator contents until the scaler is completely full. At this instant the integrator output provides the required error information. A detailed schematic of this servo system is shown in Fig. 10. The up–down counter is formed by the three 4-bit scalers D1, D2, and D3, thereby providing an essentially triangular sweep output from A7. A small fraction of the same triangular signal provides a position output signal via A8 and A9 to drive the demanded position input X_D of the system described in Sec. I.

The average position of the rocking curve is determined by taking the PMT anode current via A1, A2, and Q1 through the operational transconductance amplifier A3 to a 32-μF integrating capacitor. The polarity of the integrated current reverses, through the action of A3 and D4, each time the most significant bit of D3 changes state. At the end of each sweep the buffered integrator output provided at A4 is sampled and held by the action of A5 and A6, together with the momentary sampling current signal from Q3. In this way a cumulative error signal is added to the sweep signal in such a sense as to correct for any slow drift of the position of the centroid of the rocking curve.

A number of advantages accrue from the particular design chosen for this system. Since it is digital it exhibits no long-term drift of its own, and in addition provides a digital address at all times, corresponding to

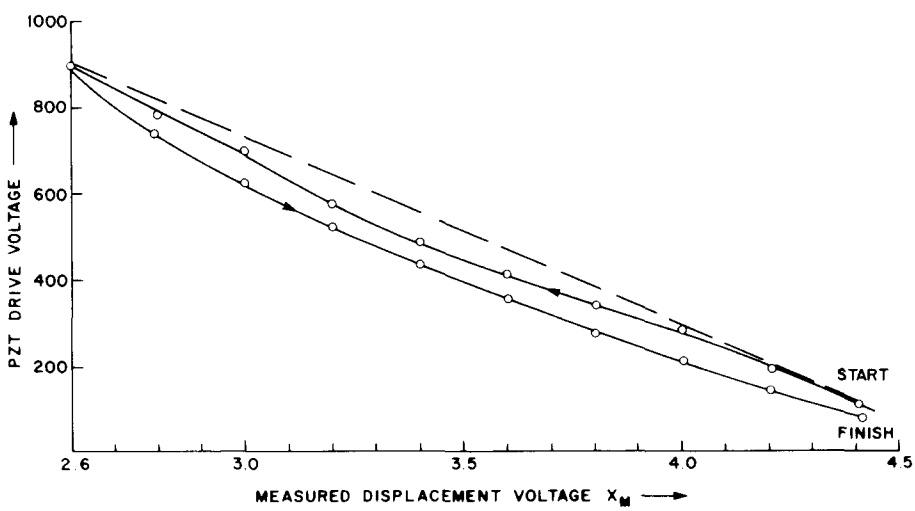

FIG. 8. Measured distance–voltage response of the PZT transducer.

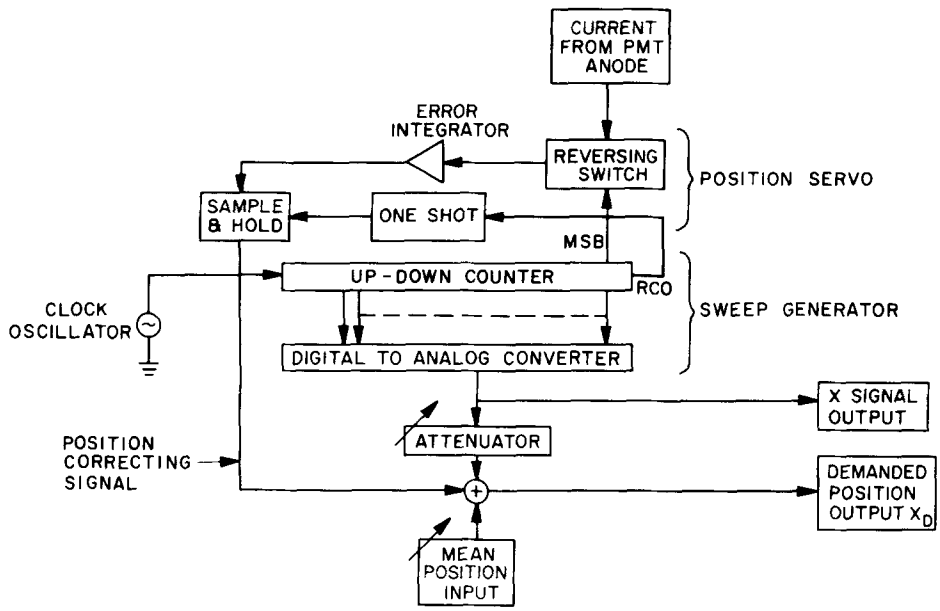

FIG. 9. Simplified block diagram of the digital sweep and servo system. The item marked "reversing switch" actually changes the sign of the signal current flowing into the error integrator on command from the up–down counter MSB.

the instantaneous value of x (from the 12 bits of D1–D3). Alternatively, the instantaneous angular position can also be provided in the form of a pulse by sampling the output of A7.

III. RESULTS

High-quality strain-free single crystals of silicon were selected for use as the monochromator and target of the system of Fig. 1. For illustrative purposes a (220) rocking curve was then taken using the PZT drive voltage itself as the X signal (i.e., the angle signal) on an $X-Y$ plotter, while the Y signal was provided by the PMT output current via A1. The result is shown in Fig. 11(a). The relative displacement of two successive to-and-from sweeps is clearly evident and is a consequence of the PZT hysteresis shown in Fig. 8.

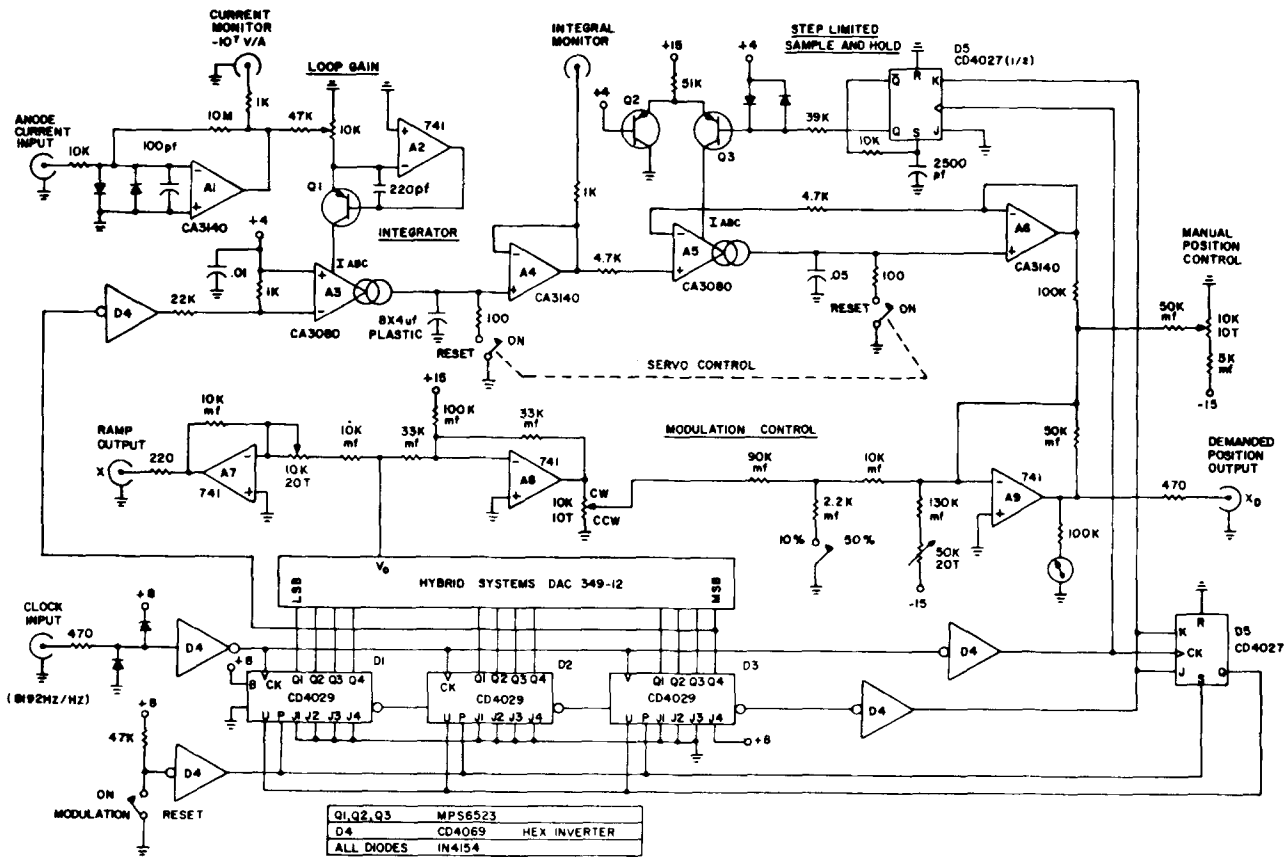

FIG. 10. Detailed schematic of the digital sweep and servo system.

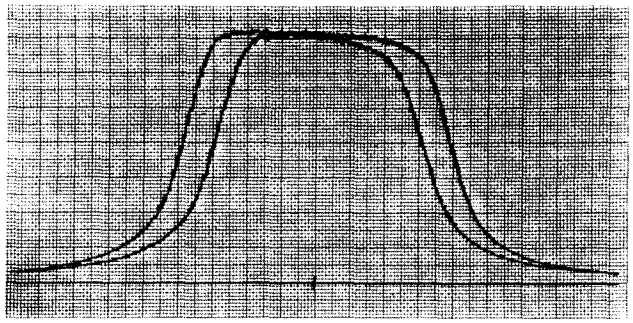

(a)

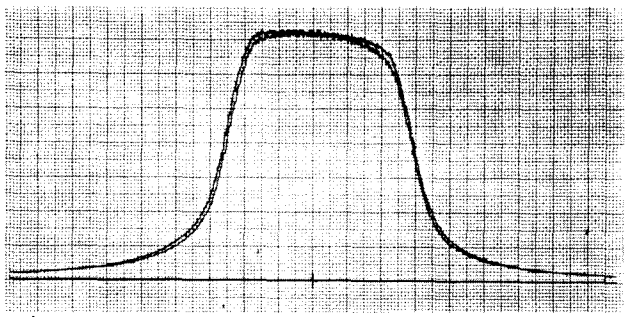

(b)

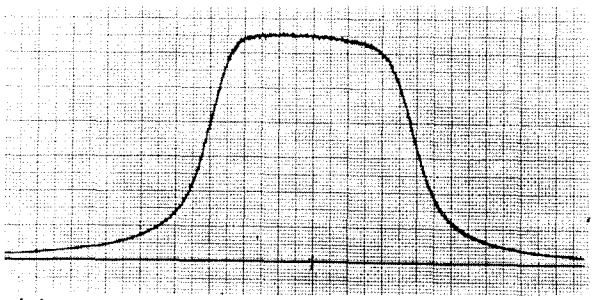

(c)

FIG. 11. (a)–(c) show Si(220) rocking curves; the ordinate is the PMT anode current (in arbitrary units) while the abscissa is proportional to the angular rotation of the sample. The FWHM of the rocking curves are $\sim 10^{-5}$ rad in all three cases. (a) uses the PZT drive voltage itself for angular information, while (b) uses the capacitor plate system. (c) shows the improvement over (b) on employing the modified goniometer design of Fig. 12.

On connecting up the capacitance sensing system of Sec. I and using this to provide the angle information instead of the PZT voltage, the results of Fig. 11(b) were obtained. While this was evidently a substantial improvement over the case of Fig. 11(a) it was also clear that some small hysteresis still remained.

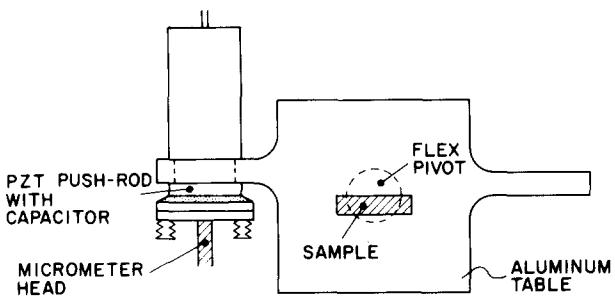

FIG. 12. Improved goniometer design with flex-pivot support.

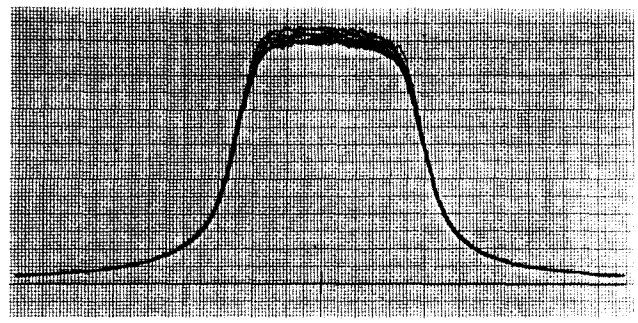

(a)

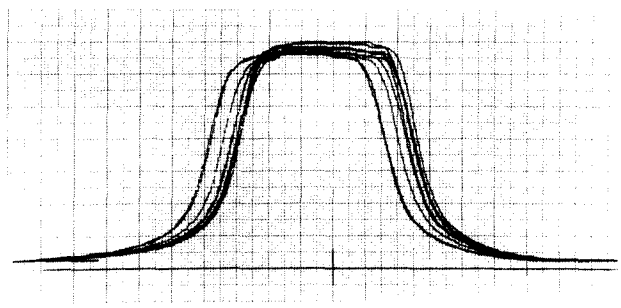

(b)

FIG. 13. (a) shows a family of Si(220) rocking curves taken at 10-min intervals over a period of 1.5 h. Since the FWHM angular width is $\sim 10^{-5}$ rad it is evident that the long-term system stability is no worse than a few percent of that figure. (b) shows the PMT anode current versus the demanded position signal over the same time period, thereby displaying the correcting action of the complete servo system.

Careful tests failed to reveal any measurable hysteresis effect in the distance measuring system itself, from which it was concluded that the origin of this phenomenon must lie elsewhere, and suspicion fell on the pivot-type goniometer used to mount the rocking crystal.

On replacing this goniometer with the simplified, but improved, design shown in Fig. 12 the results of Fig. 11(c) were obtained. It is evident that the use of a Flexpivot (Bendix type 5016-600), which employs only a mechanical flexing motion instead of any sliding or rolling action, essentially removed the remaining hysteresis effect evident in Fig. 11(b).

Of course, all three results of Fig. 11 were obtained on a short time scale, approximately 5 s per sweep, and therefore did not provide any information on the action of the servo system of Sec. II that provides long-term stabilization of the average rocking curve position.

This information was obtained by first adjusting the loop gain control of Fig. 10 to provide overall closed-loop action without overshoot or oscillation and then allowing the system to sweep continuously. The pen of the $X-Y$ plotter was dropped every 10 min to obtain data over 10 such periods, totalling 1 h and 40 min, as shown in Fig. 13. The overall angular width of this silicon (220) rocking curve is known to be $\sim 10^{-5}$ rad, indicating that the long-term angular stability of the complete servo system is no worse than a few percent of that figure, i.e., $\sim 10^{-7}$ rad.

As a further test of the system's performance rocking curve plots were also taken at the same 10-min intervals using X_D as the plotter X-input signal, instead of the ramp output signal of Fig. 10. This data is shown in Fig. 13(b) and clearly demonstrates the magnitude of the effect for which the system was correcting during the 100-min data accumulation period. The actual magnitude of the PZT sweep drive voltage for all of the results of Figs. 11 and 13 was ~40 V, while the total available swing was ~1000 V. This wide difference was intentionally allowed for in the design in order to encompass much larger total drifts than those evidenced in Fig. 13(b). Such enhanced drift effects might well be encountered in situations where data is accumulated over a period of days instead of hours.

An additional advantage of the average position servo system, is that it can accurately recenter the rocking curve following mechanical disturbances of the system. In particular, this is important since the tilt of the sample about the horizontal axis must occasionally be realigned manually.

A final point to be made regarding Fig. 13 is that no special steps were taken to stabilize either the x-ray tube intensity or the PMT gain. It is for this reason that the absolute intensity of the rocking curves shows some change with time, although this is of no significance for the purposes of the present investigations.

[1] B. W. Batterman, Phys. Rev. **133,** A759 (1964).
[2] J. A. Golovchenko, B. W. Batterman, and W. L. Brown, Phys. Rev. B **10,** 4239 (1974).
[3] S. K. Anderson, J. A. Golovchenko, and G. Mair, Phys. Rev. Lett. **37,** 1141 (1976).
[4] S. Annaka, S. Kikuta, and K. Kohra. J. Phys. Soc. Jpn. **21,** 1559 (1966).
[5] V. N. Shchemelev and M. V. Kruglov, Sov. Phys. Solid State **14,** 2988 (1973).
[6] M. T. Gladwin and J. Wolfe, Rev. Sci. Instrum. **46,** 1099 (1975).